Applied Catalysis B: Environmental 163 (2015) 531–538

Contents lists available at ScienceDirect

Applied Catalysis B: Environmental

journal homepage: www.elsevier.com/locate/apcatb

Influence of Mo on catalytic activity of Ni-based catalysts in hydrodeoxygenation of esters

R.G. Kukushkin[a,*], O.A. Bulavchenko[a], V.V. Kaichev[a,b], V.A. Yakovlev[a,b,c]

[a] Boreskov Institute of Catalysis, Lavrentieva Ave. 5, 630090 Novosibirsk, Russia
[b] Novosibirsk State University, Pirogova Str. 2, 630090 Novosibirsk, Russia
[c] UNICAT Ltd., Lavrentieva Ave. 5, 630090 Novosibirsk, Russia

ARTICLE INFO

Article history:
Received 19 May 2014
Received in revised form 26 July 2014
Accepted 2 August 2014
Available online 11 August 2014

Keywords:
Hydrodeoxygenation
Hydrocarbon
Ni-based catalysts
Biofuel

ABSTRACT

The effect of molybdenum on activity of Ni-based catalysts in the hydrodeoxygenation of fatty acid esters was studied. Catalysts Ni-Cu/Al_2O_3, Ni-Mo/Al_2O_3, Cu-Mo/Al_2O_3, Mo/Al_2O_3, and Ni-Cu-Mo/Al_2O_3 with different ratios Ni/Mo were prepared and tested in the hydrodeoxygenation of methyl palmitate and ethyl caprate at 300 °C, 1 MPa. It was found that an increase in the Mo content (from 0.0% to 6.9%) in the Ni-Cu-Mo/Al_2O_3 catalysts leads to an increase in the yield of normal alkanes. The catalysts were characterized by X-ray photoelectron spectroscopy (XPS), temperature programmed reduction and X-ray diffraction techniques. The XPS data showed that the increase in the conversion of fatty acid esters is related to changes in the ratio between different oxidation states of molybdenum (Mo^0, Mo^{4+}, and Mo^{6+}) on the surface of the Ni-Cu-Mo/Al_2O_3 catalysts.

1. Introduction

Rising demand for energy, environmental issues and depletion of oil reserves create the need to develop alternative methods of energy production from renewable sources, including biomass. The use of biofuels can help to cope with the growing energy consumption and to solve a number of environmental problems [1]. Although the use of vegetable oils as a fuel is still considered today [2], they have certain drawbacks that lead to problems in the long-term operation of internal combustion engines [3]. Analogous drawbacks, but to a lesser extent, are inherent to biodiesel, as well. The higher viscosity, cloud point, and the higher acid number of biodiesel limit its use in conventional internal combustion engines. Removing oxygen from fatty oxygenates (triglycerides of fatty acids, free fatty acids, and their esters) is an alternative route for obtaining higher quality components of motor fuels—hydrocarbons [4]. In production of biofuels, the hydrodeoxygenation (a reaction of oxygen removal from an organic substrate via hydrogenolysis) is one of the main reactions for hydrotreatment of fatty oxygenates. Linear alkanes C_{15}–C_{18} that are formed after the hydrotreatment undergo further hydroisomerization to yield either kerosene or diesel fractions, depending on conditions [5].

To date, lipids of vegetable origin are hydrodeoxygenated mainly in the presence of catalysts of two major types: sulfided catalysts for desulfurization of petroleum (Ni-Mo/Al_2O_3 and Co-Mo/Al_2O_3) and catalysts based on noble metals (Pd/C, Pt/Al_2O_3) [6–8]. For example, Pd/C catalysts were shown to be highly effective in the selective hydrodeoxygenation of ethyl stearate into alkanes [4]. The hydrodeoxygenation of methyl esters of fatty acids in the presence of a Pt/Al_2O_3 catalyst also leads to a high yield of alkanes [7]. In general, the catalysts based on noble metals are more active, but more expensive. Therefore, catalysts with the active component based on less expensive metals are of greater interest. For example, the hydrodeoxygenation of various compounds, including fatty esters of carboxylic acids, has been tested in the presence of conventional sulfided catalysts for the desulfurization: Ni-Mo/Al_2O_3 and Co-Mo/Al_2O_3 [9]. In recent studies [10], the catalyst Ni-Mo/Al_2O_3 was tested in the hydrodeoxygenation of rapeseed oil and, as in the case with the catalysts Pd/C and Pt/Al_2O_3, the major reaction products were alkanes. However, activity of sulfided catalysts in the hydrodeoxygenation reaction of esters could be lower in the absence of sulfiding agent [11–13]; to maintain catalytic activity, addition of sulfiding agent is necessary [11].

In this regard, an urgent task today is to design stable unsulfided catalysts containing no noble metals and exhibiting high activity in the hydrodeoxygenation of lipids of vegetable origin. A possible solution to this problem is the development of catalysts based on Ni. Monometallic nickel catalysts are known to be active in the hydrodeoxygenation of vegetable oils [14], while catalysts

* Corresponding author. Tel.: +7 383 326 96 52; fax: +7 383 330 62 54.
E-mail address: roman@catalysis.ru (R.G. Kukushkin).

http://dx.doi.org/10.1016/j.apcatb.2014.08.001
0926-3373/

based on Ni–Cu alloys exhibit activity in the hydrodeoxygenation of biodiesel [15]. The addition of copper also reduces the production of methane, which is an undesired by-product formed during the hydrodeoxygenation of biodiesel [15]. Besides, the addition of copper can reduce carbonization of the catalyst surface [16,17] and increase the catalyst stability against sintering of the active component [17]. Unfortunately, the addition of copper does not solve the problem of leaching of the active component of the catalyst [18], and unsulfided nickel catalysts have to be additionally modified to improve their stability and resistance to leaching. For example, nickel–molybdenum alloys are known to have higher chemical resistance to acids as compared with monometallic nickel catalysts [19,20].

Nowadays, the study of the influence of molybdenum, as modifying metal, on activity and selectivity of nickel-based catalysts in the reaction of hydrogenation of esters is of interest. An additional challenge was determination of the main correlations between the nature of the active component of catalysts and their catalytic properties. For this purpose, we prepared a series of Ni-Cu-Mo/Al_2O_3 catalysts with different molybdenum contents and studied their chemistry, structure, and catalytic performance.

2. Experimental

2.1. Materials

Ethyl caprate (Acros organics, 99+%) and methyl palmitate (Alfa Aesar, 97%) were used as received. Spherical particles of Al_2O_3 with a diameter of 1.5 mm were obtained from Sasol (Hamburg, Germany).

2.2. Catalysts preparation

Before the catalyst preparation, Al_2O_3 was calcined in air at 1000 °C.

Monometallic catalysts Ni/Al_2O_3, Mo/Al_2O_3 and Cu/Al_2O_3 were prepared by incipient wetness impregnation of calcined Al_2O_3 with an aqueous solution of $Ni(NO_3)_2{\cdot}6H_2O$, $(NH_4)_6Mo_7O_{24}{\cdot}4H_2O$ and $Cu(NO_3)_2{\cdot}3H_2O$, respectively. Bimetallic catalysts Ni-Cu/Al_2O_3, Cu-Mo/Al_2O_3, and Ni-Mo/Al_2O_3 were prepared by impregnation of Al_2O_3 with mixtures of aqueous solutions of $Ni(NO_3)_2{\cdot}6H_2O$, $Cu(NO_3)_2{\cdot}3H_2O$, and $(NH_4)_6Mo_7O_{24}{\cdot}4H_2O$ taken in corresponding pairs.

All the impregnated catalysts were dried for 5 h at 120 °C and then calcined in a muffle furnace for 6 h at 520 °C. If necessary, the impregnation procedure followed by drying and calcination was repeated.

Trimetallic catalysts Ni-Cu-Mo/Al_2O_3 were prepared by the additional impregnation of the Ni-Cu/Al_2O_3 catalyst with an aqueous solution of $(NH_4)_6Mo_7O_{24}{\cdot}4H_2O$, also followed by drying and calcination.

2.3. Catalysts characterization

The specific surface area of samples were determined with the Brunauer–Emmett–Teller (BET) method using nitrogen adsorption isotherms measured at liquid nitrogen temperatures with an automatic volumetric adsorption unit ASAP 2400 (Micromeritics Instrument. Corp., USA).

Temperature programmed reduction (H_2-TPR) of the catalysts was studied in a flow of a mixture of H_2 (10%) and Ar (90%) at the flow rate of 40 mL/min. The weight of a catalyst sample was varied depending on the metal content (m_{met} = 50 mg). Samples were placed in a U-shaped quartz reactor and heated in the reducing atmosphere at a constant heating rate of 5 °C/min up to 700 °C. Changes in the concentration of hydrogen at the reactor outlet were measured using a thermal conductivity detector (TCD).

X-ray diffraction (XRD) of the fresh catalysts was studied *ex situ* with a diffractometer X'tra (Thermo, Switzerland) using monochromatic Cu Kα radiation (λ = 154.18 pm). The diffraction patterns were recorded in steps of 0.05° with a count time of 3 s in the 2θ range of 15–70°. Before *ex situ* XRD analysis all the samples were reduced in a hydrogen flow at 520 °C and then passivated with alcohol to prevent the interaction with air. The reduction of the catalysts was studied *in situ* using synchrotron radiation facilities at the Siberian Synchrotron and Terahertz Radiation Center (Novosibirsk, Russia). The experiments were performed using a diffractometer equipped with a high-temperature reactor chamber XRK-900 (Anton Paar, Austria). The sample was loaded into the reactor on an open holder, allowing hydrogen to pass through the sample volume. The chamber was mounted to the diffractometer so that the monochromatic synchrotron radiation beam was incident on the sample surface at an angle of approximately 15°. The *in situ* X-ray diffraction patterns of the catalyst were recorded in the range of 32–61°.

The chemical composition of the catalysts was studied by X-ray photoelectron spectroscopy (XPS) using a photoelectron spectrometer (SPECS Surface Nano Analysis GmbH, Germany) equipped with a hemispherical analyzer PHOIBOS-150, an X-ray monochromator FOCUS-500, and an X-ray source XR-50M with a double Al/Ag anode. The spectrometer was also equipped with a high-pressure cell (HPC) that allowed us the heating of samples in gas mixtures at pressures up to 5 atm. The XPS spectra were recorded using monochromatic Al Kα radiation ($h\nu$ = 1486.74 eV). The binding energy (E_b) of the photoemission peaks were corrected to the $Ni2p_{3/2}$ peak (E_b = 852.70 eV) of nickel in the metallic state, which was a component of the catalysts.

Before XPS analysis all the samples were reduced in a hydrogen flow at 520 °C and then passivated with alcohol to prevent the interaction with air. Then, the samples were re-reduced at 350 °C at hydrogen pressure of 0.1 MPa for 1 h directly in HPC.

2.4. Catalysts performance

The catalyst performance was tested in a steel fixed-bed reactor at 1 MPa, 300 °C. The feed rates of the carrier gas (Ar) and hydrogen were 15 and 5 L/h, respectively. A mixture of methyl palmitate and ethyl caprate was used as a substrate. The substrate feed rate U was 3 mL/h, the LHSV was 3 h^{-1}, the catalyst volume was V_{cat} = 1 cm^3. Before the experiments, catalysts (fraction 0.2/0.5 mm) were reduced in the reactor at 520 °C in a hydrogen flow at 0.1 MPa for 1 h. After that, the reactor was cooled to a desired temperature and the substrate was added to the feed. The liquid phase was sampled not rarer than once per hour.

2.5. Analysis of reaction products

The product composition was analyzed in the liquid phase using a GC–MS spectrometer Agilent Technologies 7000B equipped with a quartz capillary column HP-5ms (stationary phase: 5% phenyl + 95% dimethylpolysiloxane, length 30 m, inner diameter 0.25 mm). The quantitative analysis of the liquid products was carried out using a chromatograph GC Chromos 1000 equipped with a capillary column Zebron ZB-5 (stationary phase: 5% phenyl + 95% dimethylpolysiloxane, length 30 m, internal diameter 0.32 mm, phase thickness 0.25 μm). The gas phase (H_2, CO, CO_2, and CH_4) was analyzed with a chromatograph GC Chromos 1000 equipped with a flame ionization detector and TCD and with a column packed with silochrome and activated charcoal (length 3 m, inner diameter 2 mm).

Table 1
The specific surface area and composition of the catalysts before reducing treatment.

Catalyst	Composition			S_{BET} (m^2/g)
	Ni	Cu	Mo	
Ni-Cu/Al_2O_3	13	5		118
Ni-Cu-2.2Mo/Al_2O_3	12.4	4.8	2.2	114
Ni-Cu-3.9Mo/Al_2O_3	11.7	4.5	3.9	110
Ni-Cu-5.6Mo/Al_2O_3	11.3	4.3	5.6	103
Ni-Cu-6.9Mo/Al_2O_3	10.1	3.8	6.9	100
Mo/Al_2O_3			7	123
Cu-Mo/Al_2O_3		6	10	117
Ni-Mo/Al_2O_3	9		11	116
Ni/Al_2O_3	9.6			125

2.6. Measurement of catalyst performance

The catalyst efficiency was evaluated according to both conversion X (mol%) of the initial substrate and degree of hydrodeoxygenation (HDO), which were calculated as follows:

$$X = \left(1 - \frac{n}{n_0}\right) \times 100\%,$$

and

$$\text{HDO} = \frac{\sum n_i'}{\sum n_i} \times 100\%.$$

Here, n is the amount of unreacted esters (mole), n_0 the initial amount of ester (mole), $\sum n_i'$ the sum of moles of products that do not contain oxygen, and $\sum n_i$ is the sum of moles of all products.

Selectivity S_i toward a product ***i*** was determined as a percent of this product in the liquid phase, here $\sum n_i$ is the sum of moles of all products.

$$S_i = \left(\frac{n_i}{\sum n_i}\right) \times 100\%.$$

The total yield of alkanes is then defined as:

$$\text{yield of alkanes} = S_{\text{alkanes}} \times X$$

3. Results and discussion

3.1. Catalysts characterization

Results of the elemental analysis of freshly prepared catalysts and their specific surface areas (BET) are shown in Table 1.

3.1.1. Temperature-programmed reduction

The temperature-programmed reduction of catalysts showed that the Ni/Al_2O_3 catalyst exhibited three peaks of hydrogen absorption: at 250, 450, and 640 °C (Fig. 1). The first low-temperature peak at 250 °C was attributed to the reduction of Ni (III) [21], which was formed during oxygen chemisorption. The main form, NiO, was reduced at 450 °C, while the peak at 640 °C was attributed to the reduction of surface $NiAl_2O_4$. The last feature in the TPR profiles of Ni/Al_2O_3 pointed to a strong interaction between the deposited metal and the alumina support. Fig. 1 also demonstrates the H_2-TPR profiles of the catalysts Ni-Cu/Al_2O_3, Ni-Mo/Al_2O_3, Cu-Mo/Al_2O_3, and Ni-Cu-Mo/Al_2O_3 with the different Mo content. The profiles for the monometallic systems Cu/Al_2O_3 and Mo/Al_2O_3 are shown for comparison.

As seen from Fig. 1, the Ni-Cu/Al_2O_3 catalyst exhibited three major peaks of hydrogen absorption with the maximums at 220, 365, and 525 °C. As compared with the Ni/Al_2O_3 catalyst, the peaks of Ni-Cu/Al_2O_3 were shifted toward lower temperatures. The reason for this effect is discussed in detail elsewhere [22]. In fact it is determined by lower molar free energy of reduction of CuO in comparison with NiO. Most of hydrogen for the catalysts Ni-Mo/Al_2O_3, Mo/Al_2O_3 and Ni/Al_2O_3 was absorbed in the same temperature range 450–600 °C (Fig. 1). In the case of the Mo/Al_2O_3 catalyst, hydrogen absorption peak observed at 470 °C corresponds to the reduction of MoO_3 to MoO_2. The increase of the hydrogen absorption observed after 650 °C apparently corresponds to the reduction of MoO_2 to Mo^0, it is consistent with results of recent studies [23,24]. In the case of Ni-Mo/Al_2O_3 as in the case of Mo/Al_2O_3 major absorption peak of hydrogen observed at approximately 480 °C, however, after 520 °C absorption of hydrogen remains elevated, that probably indicates that the MoO_2 reduction in the presence of nickel begins at lower temperatures. In contrast, the H_2-TPR profile of Cu-Mo/Al_2O_3 did not contain the peak at 450–550 °C that is typical of Mo/Al_2O_3. Therefore, it may be assumed that the calcination of Cu-Mo/Al_2O_3 led to the formation of a new phase containing copper and molybdenum, which was reduced at lower temperatures (250–350 °C). This apparently indicates the formation of a Cu-Mo phase and the influence of Cu^0 on reduction of Mo^{6+} to Mo^{4+}.

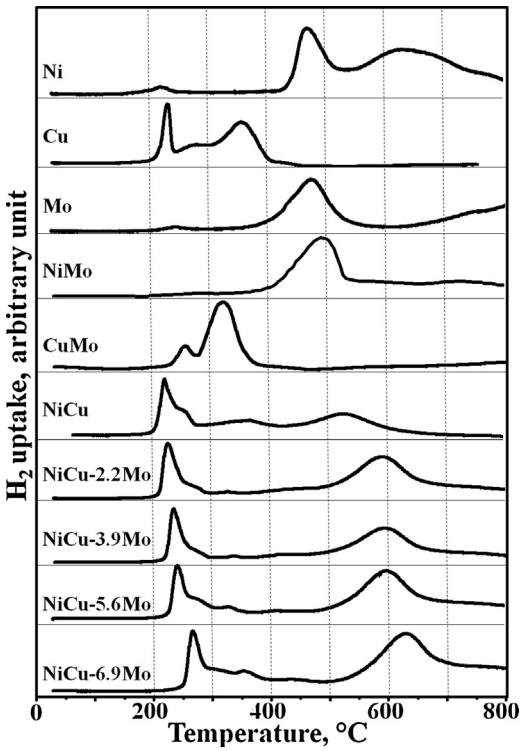

Fig. 1. H_2-TPR profiles of catalysts Ni/Al_2O_3, Cu/Al_2O_3, Mo/Al_2O_3, Ni-Cu/Al_2O_3, Ni-Mo/Al_2O_3, Cu-Mo/Al_2O_3, and Ni-Cu-Mo/Al_2O_3 with the different Mo content.

The H_2-TPR profiles of catalysts Ni-Cu-Mo/Al_2O_3 showed that an increase in the Mo content led to a shift of the main peaks toward higher temperatures as compared with the catalyst Ni-Cu/Al_2O_3. The shift was detected both for the low-temperature peak at 220–280 °C and for the peak at 550–650 °C. This effect may be attributed to the formation of trimetallic Ni-Cu-Mo phases.

3.1.2. X-ray diffraction

The catalysts Ni-Cu/Al_2O_3 and Ni-Cu-Mo/Al_2O_3 reduced at 520 °C and treated with ethanol were studied by XRD. All the samples exhibited peaks due to the phases of metallic nickel and copper. In addition, the samples Ni-Cu-5.6Mo/Al_2O_3 and Ni-Cu-6.9Mo/Al_2O_3 showed peaks due to the phase of MoO_2, which possibly appeared because of the higher Mo content of these catalysts and because of the partial reduction of Mo^{6+} to Mo^{4+} (Table 2).

Table 2
Lattice parameters of reduced catalysts. The samples were reduced at 520 °C and treated with ethanol.

Sample	Phase composition	Lattice parameter (Å)
Ni-Cu/Al_2O_3	Ni*	3.549
	Cu*	3.599
Ni-Cu-2.2Mo/Al_2O_3	Ni*	3.556
	Cu*	3.604
Ni-Cu-3.9Mo/Al_2O_3	Ni*	3.552
	Cu*	3.606
Ni-Cu-5.6Mo/Al_2O_3	MoO_2	
	Ni*	3.555
	Cu*	3.611
Ni-Cu-6.9Mo/Al_2O_3	MoO_2	
	Ni*	3.558
	Cu*	3.610
Cu-Mo/Al_2O_3	Cu*	3.616
	Cu_2O	
	MoO_2	
Ni-Mo/Al_2O_3	Ni*	3.562

* Reference data for the lattice parameter: Ni, 3.523 Å [PDF # 040850]; Cu, 3.615 Å [PDF # 040836].

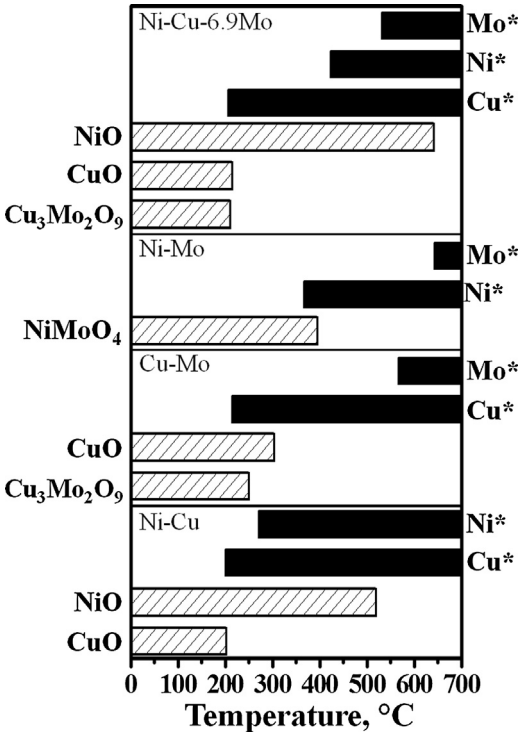

Fig. 2. Changes in the phase composition of catalysts Cu-Mo/Al_2O_3, Ni-Mo/Al_2O_3, Ni-Cu-6.9Mo/Al_2O_3, and Ni-Cu/Al_2O_3 during *in situ* reduction with hydrogen. Heating rate was 5 °C/min. The XRD patterns were taken with the frequency of 1 frame per 2 min.

As seen from Table 2, the experimentally obtained lattice parameters of metallic Ni and Cu differed from the reference data (Cu, 3.615 Å; Ni, 3.523 Å). It indicates the inclusion of Mo and Cu atoms into the crystal lattice of Ni and hence the formation of solid solutions. The bimetallic Ni-Cu sample contained solid solutions with the composition of $Ni_{1-x}Cu_x$. In the catalysts Ni-Cu-Mo/Al_2O_3, the formation of solid solutions of more complex composition, with the inclusion of Mo atoms, is possible. For the systems containing Mo (Ni-Cu-Mo/Al_2O_3), it was difficult to determine the composition of metallic compounds by XRD because the addition of Cu and Mo atoms into the structure of Ni should have increased the lattice parameter and it was impossible to distinguish the contribution of each element. Nevertheless, the fact that lattice parameters obtained for the Ni-systems differed from those for Ni-Mo-systems indirectly indicated the possible formation of a solid solution.

The study of the sample Ni-Cu/Al_2O_3 by *in situ* XRD in a dynamic mode, during an increase of the reduction temperature, showed that copper oxide was reduced to the metal at temperatures below 200 °C. Presumably, reduced copper diffused into the crystal lattice of nickel oxide, thereby helping to decrease the degree of oxidation of nickel and, consequently, to reduce nickel at lower temperatures. Nickel in this catalyst existed both in the oxide form and in the metallic state in a wide temperature range (270–520 °C). The increase in the lattice parameter of Ni (Table 2) it the completely reduced samples indicated the formation of solid solutions with the composition of Ni_xCu_{1-x}. The modification of the Ni-Cu system with molybdenum oxide led to the appearance of a new phase $Cu_3Mo_2O_9$, which corresponds to the assumption based on the H_2-TPR data. This phase was reduced simultaneously with CuO at 200 °C to form metallic copper. However, the reduced state Mo^0 appeared at higher temperatures. During the reduction of Ni-Cu-6.9Mo/Al_2O_3 and Cu-Mo/Al_2O_3, the phase Mo^0 was formed above 540 and 560 °C, respectively, whereas in the case of Ni-Mo/Al_2O_3, this phase was formed only above 640 °C. Below these temperatures, molybdenum existed apparently in an X-ray amorphous oxide state. Presumably, the reduction temperatures of molybdenum oxides differed because of the presence of metallic copper, which facilitated the reduction of Mo oxides. In the case of Ni-Mo/Al_2O_3, the calcination led to the formation of the oxide phase $NiMoO_4$, which was reduced only at 400 °C to form metallic Ni and molybdenum oxides, which becomes X-ray amorphous because of changes in its structure (Fig. 2).

3.1.3. X-ray photoelectron spectroscopy

All the catalysts apart from Ni/Al_2O_3 and Cu/Al_2O_3 were studied by XPS after reduction in hydrogen. It is allowed us to determine the chemical state of metals and the atomic ratios of elements in the near-surface layers of the catalysts where the catalysis takes place. The corresponding atomic ratios are present in Table 3.

As can be seen from Table 3 the atomic ratio [O]/[Al] was close to stoichiometric. The ratios [Ni]/[Al] and [Cu]/[Al] were in the range 0.06–0.08 and 0.03–0.09, respectively. The atomic ratio [Mo]/[Al] for the catalysts Ni-Cu-2.2Mo/Al_2O_3-Ni-Cu-6.9Mo/Al_2O_3 increased from 0.015 to 0.069, respectively, which is the result of the increase in the molybdenum content.

Fig. 3a shows the Ni2p spectra of the catalysts. The spectra contains two sharp high-intensive peaks at 852.7 and 869.9 eV corresponded to the $Ni2p_{3/2}$–$Ni2p_{3/2}$ spin–orbit doublet. These binding energies are typical of nickel in the metallic state [25]. It means that nickel in the near-surface layers of the catalysts mainly reduced to the metallic state after the treatment in hydrogen. Other low-intensive peaks at 856 and 874 eV are attributed to Ni(II) species [26]. It is in good agreement with H_2-TPR data (Fig. 1) which indicate the presence of surface $NiAl_2O_4$ reduced at 640 °C only.

Fig. 3b demonstrates the Cu2p spectra of the same catalysts. All spectra consist of two sharp peaks corresponded to components of the $Cu2p_{3/2}$ spin–orbit doublet. Taking into account values of the $Cu2p_{3/2}$ binding energy and the Auger parameter α, which is equal to the sum of the $Cu2p_{3/2}$ binding energy and the Cu*LMM* kinetic energy [27], we can speculated that copper in the catalysts exists in the metallic state mainly. Indeed, such Cu2p spectra without high-intensive shake-up satellites are typical of copper in both of the Cu^0

Table 3
Relative atomic concentrations of elements in the near-surface layer of reduced catalysts determined by XPS.

Sample	[Ni]/[Al]	[Mo]/[Al]	[Cu]/[Al]	[O]/[Al]
Ni-Mo	0.03	0.04	–	1.6
Ni-Cu	0.08	–	0.04	1.5
Cu-Mo	–	0.07	0.09	1.4
Ni-Cu-2.2Mo	0.08	0.015	0.05	1.2
Ni-Cu-3.9Mo	0.08	0.032	0.05	1.4
Ni-Cu-5.6Mo	0.07	0.050	0.04	1.5
Ni-Cu-6.9Mo	0.06	0.069	0.03	1.5

Table 4
Content of different forms of Mo in the near-surface layers of catalysts Cu-Mo/Al_2O_3, Ni-Mo/Al_2O_3, and Ni-Cu-Mo/Al_2O_3 reduced at 520 °C in a hydrogen flow.

Sample	Content of different forms of Mo (%)		
	Mo^0	Mo^{4+}	Mo^{6+}
Ni-Mo	57	29	14
Ni-Cu-2.2Mo	49	14	37
Ni-Cu-3.9Mo	48	21	31
Ni-Cu-5.6Mo	39	34	27
Ni-Cu-6.9Mo	37	38	25
Cu-Mo	6	49	45

and Cu^{1+} states [22]. However, bulk metallic copper is characterized by the Auger parameter equal to 1851.4 eV whereas Cu_2O is characterized by the Auger parameter equal to 1849.4 eV [28]. In our case, α is equal to 1851.1 ± 0.1 eV.

In contrast to nickel and copper, molybdenum was only partially reduced by hydrogen. The Mo3d spectra of the catalysts Ni-Cu-Mo/Al_2O_3 exhibited three doublets $Mo3d_{5/2}$-$Mo3d_{3/2}$ with the $Mo3d_{5/2}$ binding energies near 227.9–228.2, 229.4–229.6, and 232.5–232.6 eV (Fig. 3c). These binding energies correspond to Mo in the metallic state Mo^0 and in the oxidized states Mo^{4+} and Mo^{6+}, respectively. In the near-surface layers of these catalysts, the fraction of molybdenum reduced to the metallic state was from ~50% to ~37% for Ni-Cu-2.2Mo/Al_2O_3 and Ni-Cu-6.9Mo/Al_2O_3, respectively (Table 4).

Analysis of the relative intensities of the XPS peaks made it possible to determine the amount of different forms of Mo on the surface, depending on the catalyst composition. The relatively high content of Mo^0 found in the catalyst Ni-Mo/Al_2O_3 was related to distinctions in its preparation. The simultaneous deposition of molybdenum and nickel salts from the impregnating solution facilitated the formation of the $NiMoO_4$ phase in the unreduced catalysts. Interaction of oxide forms of Ni and Mo facilitated the reduction of molybdenum oxides into Mo^0 with the formation of a solid solution Ni-Mo.

The XRD data obtained for the catalyst Cu-Mo/Al_2O_3 also demonstrated the formation of a mixed oxide, with the composition of $Cu_3Mo_2O_9$ (Fig. 2). As it was mentioned above, the appearance of the peak of copper molybdenum phase reduction on the Cu-Mo/Al_2O_3 TPR profile was detected. However, according to the XRD (Fig. 2) Mo metal phase was found after 560 °C only, and oxides of molybdenum in the temperature range from 250 up to 560 °C was not found, that indicating they become X-ray amorphous. Apparently, molybdenum oxides are in an X-ray amorphous state after a partial reduction of $Cu_3Mo_2O_9$ phase, which stabilized agglomerates of Cu^0. In some works it is shown that in the first stage MoO_3 reduce to MoO_2, then MoO_2 reduce to Mo^0 [23,24,29]. MoO_2 is a stable intermediate required higher temperatures for reduction than MoO_3 [24,29]. According to the TPR and XPS data, it could be assumed that copper helps for reduction of Mo^{6+} to Mo^{4+} at lower temperatures (Table 4).

Table 4 demonstrates that an increase in the Mo content in the Ni-Cu-Mo catalysts corresponded to a decrease in the content of Mo^0 and Mo^{6+} and increase of Mo^{4+} on the Ni-Cu-Mo catalyst surface. According to TPR, the increase of the molybdenum content in the Ni-Cu-Mo catalysts leads to a gradual shift of the hydrogen absorption peaks to a high-temperature region in comparison with the Ni-Cu sample, which may indicate of a formation of trimetal oxide phases. This effect is described for bimetallic phase Ni-Mo elsewhere [24]. Earlier it was shown that an increase of Mo/Ni ratio in Ni-Mo-B catalysts leads to an increase of the ratio Mo^{4+}/Mo^{6+} on the surface [30]. From the other hand, the XPS data show that an increase of the total Mo content in the catalysts leads to a decrease of the Mo^0 content in the catalysts reduced at 520 °C. Thus, the data TPR and XPS are in full agreement. Hence, the ratio of $Mo^0/Mo^{4+}/Mo^{6+}$ could be changed by varying of the Mo content and the ratios Ni/Cu/Mo. Determination of correlation between $Mo^0/Mo^{4+}/Mo^{6+}$ ratio and catalytic activity

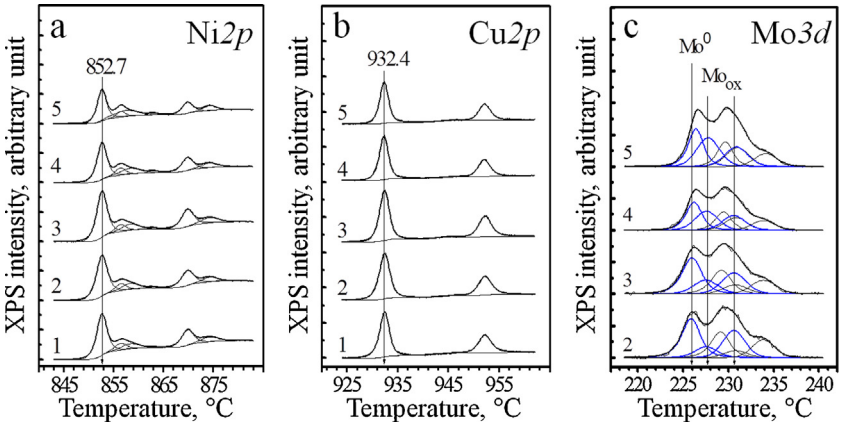

Fig. 3. Ni2p (a), Cu2p (b), and Mo3d (c) core-level spectra of reduced catalysts Ni-Cu/Al_2O_3 (1), Ni-Cu-2.2Mo/Al_2O_3 (2), Ni-Cu-3.9Mo/Al_2O_3 (3), Ni-Cu-5.6Mo/Al_2O_3 (4), and Ni-Cu-6.9Mo/Al_2O_3 (5).

Table 5
Conversion and product selectivity in the hydrodeoxygenation of a mixture of ethyl caprate and methyl palmitate in the presence of different catalysts at 300 °C, P_{H_2} = 0.25 MPa and LHSV = 3 h^{-1}.

Catalyst	Product selectivity (%)								Conversion (%)
	Alkanes[a]	C_9H_{20}	$C_{10}H_{22}$	$C_{15}H_{32}$	$C_{16}H_{34}$	Aldehydes[b]	Alcohols[c]	Esters[d]	
Ni-Cu	2	33	1.5	44.3	1.3	2.6	0.8	14	60
Ni-Cu-2.2Mo	1.5	33.2	1.7	48	1.3	0.2	0.6	13	63
Ni-Cu-3.9Mo	1.5	43	3.6	40	3.5	0.3	0.5	6.8	78
Ni-Cu-5.6Mo	1.2	38	5.2	43	4	0.4	0.15	7.6	81
Ni-Cu-6.9Mo	1.2	44	7	37	4.5	0.6	0,1	4.8	90
Ni-Mo	1.5	16	33	15	21	6.8	–	6.3	90
Mo	–	–	0.4	–	0.5	0.3	–	98	18

[a] Alkanes: C_6H_{14}–C_8H_{18}, $C_{11}H_{24}$–$C_{14}H_{30}$.
[b] Decanal, hexadecanal.
[c] 1-Hexadecanol; 1-decanol.
[d] "Exchange" esters: decanoic acid methyl ester, hexadecanoic acid ethyl ester.

allows us to make an assumption about the nature of the active centre.

3.2. Hydrodeoxygenation of ethyl caprate and methyl palmitate

After pre-reduction at 520 °C, the catalysts were tested in the hydrodeoxygenation of a mixture of ethyl caprate and methyl palmitate in a fixed bed reactor at 300 °C, P_{H_2} = 0.25 MPa and LHSV = 3 h^{-1}. The tests showed that the conversion of the ester mixture was the lowest in the presence of the Mo/Al_2O_3 catalyst, and the degree of HDO in this case did not exceed 1%. Nevertheless, although the catalyst Mo/Al_2O_3 was not active in the hydrodeoxygenation, it had the ability to catalyze the metathesis of alkyl groups of the esters (Table 5). Methyl palmitate and ethyl caprate over this catalyst were transformed into methyl caprate and ethyl palmitate. Because these esters were not formed in the presence of Al_2O_3, it may be assumed that the exchange of alkyl groups proceeded at the surface of molybdenum oxide, which indicates its ability to activate oxygen-containing compounds of this type.

Among the catalysts $Ni-Cu/Al_2O_3$ and $Ni-Cu-Mo/Al_2O_3$, the lowest conversion and the degree of hydrodeoxygenation were observed in the presence of $Ni-Cu/Al_2O_3$. Analysis of the products showed that in the presence of all these catalysts, major products were alkanes (primarily normal alkanes: nonane and pentadecane). In addition, the products contained the "exchange" esters, small amounts of alcohols and aldehydes, which were obviously hydrodeoxygenation intermediates (Table 5). Trace of ethanol and small amounts (less than 1%) of decyl caprate—the product of transesterification of ethyl caprate and decanol also were found. In the case of the $Ni-Cu/Al_2O_3$ catalyst, trace of decanoic and hexadecanoic acids were found as well.

An increase of the molybdenum content in the $Ni-Cu-Mo/Al_2O_3$ catalysts leads to an increase selectivity toward alkanes n-$C_{10}H_{22}$ and n-$C_{16}H_{34}$ (Table 5), which are the products of appropriate ethers ethyl caprate ($C_9H_{19}COOC_2H_5$) and methyl palmitate ($C_{15}H_{31}COOCH_3$) hydrogenation. In the presence of the $Ni-Mo/Al_2O_3$ catalyst selectivity toward these alkanes was the maximum. Among oxygen-containing products esters, aldehydes, as well as traces of ethanol were found.

On the basis of literature data and the obtained product distribution, a scheme of aliphatic esters conversion in the presence of nickel-containing catalysts was proposed (Fig. 4). As shown by Senol et al. [31], the formation of alkanes during the hydrodeoxygenation of esters can proceed via three major routes. In the first route, formed alcohols undergo further dehydration to olefins, which are subsequently hydrogenated to alkanes. A second route is the formation of carboxylic acids that are then converted into hydrocarbons [32] either directly or through alcohols as intermediates. The third route leads to the formation of hydrocarbons via decarboxylation. Recently [33], Monier et al. studied the hydrodeoxygenation of oleic acid. They supposed that the formation of alkanes from oleic acid can also proceed via three routes: via the hydrodeoxygenation with the formation of H_2O, via the hydrodecarbonylation with the formation of CO and H_2O, and via the hydrodecarboxylation with the formation of CO_2. In the presence of nickel-containing catalysts, CO_2 could be hydrogenated to

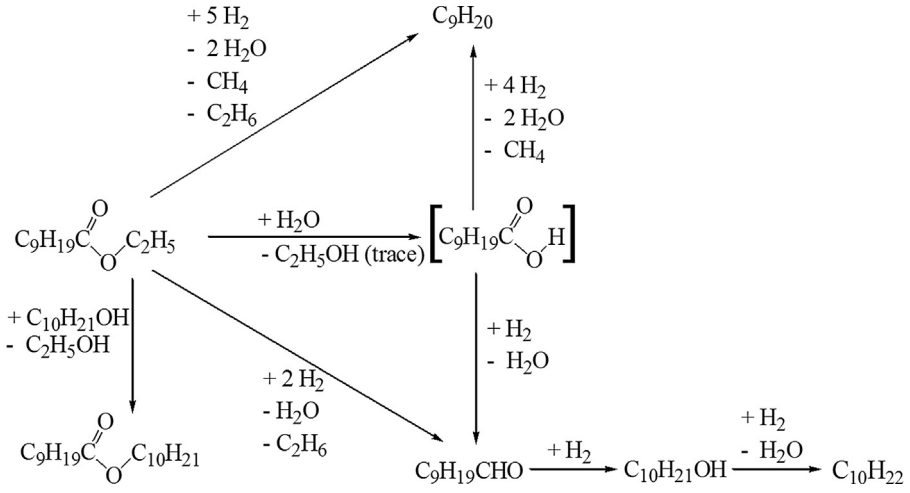

Fig. 4. A possible scheme of product formation during ester hydrodeoxygenation as illustrated by reaction of ethyl caprate in the presence of $Ni-Cu/Al_2O_3$ and $Ni-Cu-Mo/Al_2O_3$ at 300 °C, P_{H_2} = 0.25 MPa and LHSV = 3 h^{-1}.

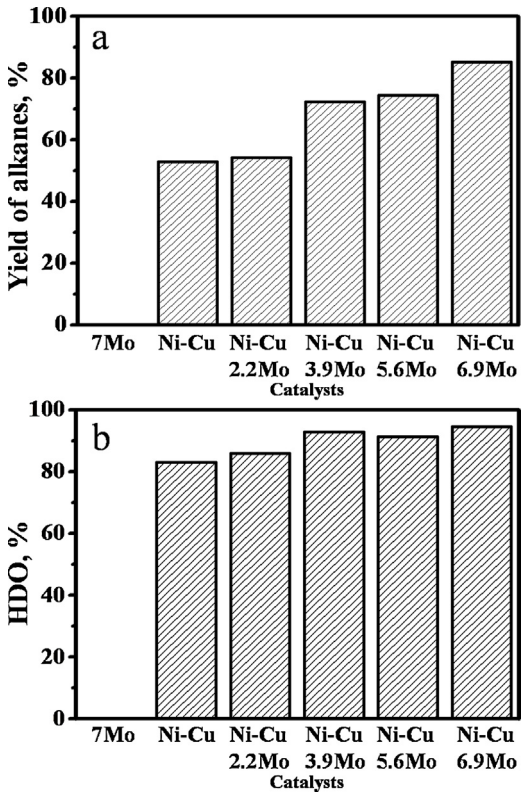

Fig. 5. Yield of alkanes (a); and degree of hydrodeoxygenation (b) in the presence of Mo/Al_2O_3, $Ni-Cu/Al_2O_3$, and $Ni-Cu-Mo/Al_2O_3$ at 300 °C, P_{H_2} = 0.25 MPa and LHSV = 3 h^{-1}.

methane [34,35], that is the reason for the absence in the gas phase CO_2 in this cycle of experiments.

In our experiments, in addition to alkanes, products contained small amounts of alcohols and aldehydes. Because traces of organic acids were found only in the presence of $Ni-Cu/Al_2O_3$, the formation of aldehydes from the ester in the presence of Ni-Cu-Mo catalysts may be considered a one-step reaction. Formation of alkanes with a chain equal to the initial acid proceed via the rupture of the C–O σ-bond of ester with the formation of the corresponding aldehyde and its subsequent reduction to alcohol, then alcohol turns into alkane either through the direct hydrogenation, or through the dehydration followed by the hydrogenation of olefins. The proposed scheme (Fig. 4) also contains a step of a subsequent transesterification of this alcohol with initial esters to give waxes. The formation of alkanes with a chain of one carbon shorter than in the initial acid was assumed to proceed mainly via the rupture of the C–C bond and cleavage of the carboxyl group bonded to the methyl group ($-COOC_2H_5$) and its subsequent destruction into two molecules of methane and ethane. Taking into account the products distribution in the presence of Ni-Cu and Ni-Cu-Mo catalysts, the decarboxylation is considered the main route of the reaction. However, as it can be seen from Table 5, an increase of the Mo content in the Ni-Cu-Mo catalysts leads to increase of the selectivity toward aldehydes and alkanes with chain length equal to the length of the chain of initial fatty acid residue. Also in the presence of catalysts $Ni-Cu/Al_2O_3$, $Ni-Cu-Mo/Al_2O_3$, and $Ni-Mo/Al_2O_3$ relatively low number of more lights alkanes - products of the hydrocracking of alkanes C_9H_{20}, $C_{10}H_{22}$, $C_{15}H_{32}$, and $C_{16}H_{34}$ are formed.

Fig. 5 shows the degree of deoxygenation and the yield of alkanes in the presence of each of the $Ni-Cu-Mo/Al_2O_3$ catalysts. As shown above, Mo by itself exhibited no activity in the hydrodeoxygenation. However, as seen, the increase in the mass fraction of Mo from 0.0 to 6.9 wt% led to an increase both in the degree of deoxygenation and in the yield of target products—normal alkanes. Therefore, the increase in activity of the Ni-Cu catalyst after its modification with Mo can be explained by the activity of oxide forms Mo^{4+} and Mo^{6+}, whose presence on the catalyst surface was confirmed by XPS and XRD (Table 4). The ability of metal oxides to activate oxygen-containing organics is attributed to the interaction of surface oxygen vacancies with the oxygen atom from the substrate molecule [36,37].

After the treatment in H_2 at 520 °C, the surface of the $Ni-Cu-Mo/Al_2O_3$ catalysts contained not only reduced molybdenum Mo^0, but also the oxide forms Mo^{4+} and Mo^{6+}. According to XPS, an increase in the mass fraction of molybdenum led to an increase in the amount of Mo^{4+} on the catalyst surface (Table 4). The XRD data (Table 2) showed that the catalysts with the highest content of Mo ($Ni-Cu-Mo5.6/Al_2O_3$ and $Ni-Cu-Mo6.4/Al_2O_3$) contained the phase MoO_2. In [38], the activity of MoO_2 and MoO_3 was tested in the hydrodeoxygenation of 4-methylphenol. It was found that the surface of MoO_2 contains mainly Mo^{4+}, while Mo^{5+} and Mo^{6+} are present in smaller amounts. The surface of MoO_3 contains only Mo^{6+}. During the reaction, MoO_3 undergoes reduction to form Mo_4O_{11}, MoO_2, and Mo^0. The activation energy of the reaction increases in the row $MoS_2 < MoO_2 < MoO_3$, whereas TOF decreases in the row $MoS_2 > MoO_2 > MoO_3$. In our case, the observed increase in the yield of alkanes may be attributed to an increase in the fraction of Mo^{4+} on the surface, which probably may explain the difference in the activation energy and hence in the catalytic activity. In [36], Pestman showed that the deposition of Pt on metal oxides increases the conversion of acetic acid during its hydrogenation because of the "spill-over" of hydrogen from Pt onto the metal oxide. Apparently, in our case, hydrogen partially migrated from the surface of Ni-Cu onto Mo, which also facilitated the transformation of esters on the molybdenum surface into alkanes.

It was shown that Ni-Mo-B catalyst with higher content of MoO_2 on the surface showed higher activity in the HDO reaction of phenol [30]. The authors noted that MoO_2 could be existed as a Mo–OH Brønsted acid cites and able to activate the C-O σ-bond. Nickel and boron in this catalyst are responsible for the activation of dihydrogen [39]. It could explain the increase of the $C_{10}H_{22}$ and $C_{16}H_{34}$ alkanes selectivity, with Mo^{4+} form increasing in our case (Table 5).

The following correlation considering the Ni-Cu-Mo catalysts could be noted: the increase of the deoxygenation degree, and, as a consequence, the increase of alkanes yield, are connected with the increase of the content of Mo^{4+} on the catalysts surface.

4. Conclusions

1. The hydrodeoxygenation of carboxylic acid esters has been studied in the presence of catalysts $Ni-Cu-Mo/Al_2O_3$ with the different Mo content. The reaction was carried out in a flow-type fixed-bed reactor at 300 °C, at partial hydrogen pressure of P_{H_2} = 0.25 MPa, and at LHSV = 3 h^{-1}. The main products were products of complete deoxygenation of esters—alkanes. A scheme for the conversion of methyl esters, which takes into account the formation of selective hydrogenation products — aldehydes and alcohols — was suggested.
2. The study of reduced catalysts $Ni-Cu-Mo/Al_2O_3$ by XRD and XPS showed that molybdenum in these catalysts exists in three states: Mo^0, Mo^{4+}, and Mo^{6+}. It was supposed that Mo^{4+} additionally activates an oxygen-organic substrate and this is one of the reasons for the improved catalytic activity of the tested $Ni-Cu-Mo/Al_2O_3$ catalysts. The obtained XRD data demonstrated that the reduction of the catalysts led to the formation of metal solid solutions, containing Ni and Cu (for $Ni-Cu/Al_2O_3$) and Ni, Cu, Mo (for $Ni-Cu-Mo/Al_2O_3$), which also could contributed to the activity of modified catalysts.

3. The deoxygenation degree and alkanes yield correlate with the Mo^{4+} form content on the Ni-Cu-Mo catalysts surface.

Acknowledgments

The work is supported by the Ministry of Education and Science of the Russian Federation. The authors acknowledge the financial support of RFBR (Russia) through grant no 14-03-31844 and UNI-HEAT project of the Skolkovo Foundation (Agreement No. 64).

References

[1] R. Luque, L. Herrero-Davila, J.M. Campelo, J.H. Clark, J.M. Hidalgo, D. Luna, J.M. Marinas, A.A. Romero, Energy Environ. Sci. 1 (2008) 542–564.
[2] F. Jiménez Espadafor, M. Torres García, J. Becerra Villanueva, J. Moreno Gutiérrez, Transport. Res. Part D: Transport Environ, 14 (2009) 461–469.
[3] F. Ma, M.A. Hanna, Bioresour. Technol. 70 (1999) 1–15.
[4] I. Kubičková, M. Snåre, K. Eränen, P. Mäki-Arvela, D.Y. Murzin, Catal. Today 106 (2005) 197–200.
[5] T.V. Choudhary, C.B. Phillips, Appl. Catal. A: Gen. 397 (2011) 1–12.
[6] A.F. Pérez-Cadenas, F. Kapteijn, M.M.P. Zieverink, J.A. Moulijn, Catal. Today 128 (2007) 13–17.
[7] P.T. Do, M. Chiaperro, L.L. Lobban, D.E. Resasco, Catal. Lett. 53 (2009) 820–829.
[8] M. Snåre, I. Kubičková, P. Mäki-Arvela, D. Chichova, K. Eränen, D.Y. Murzin, Fuel 87 (2008) 933–945.
[9] E. Furimsky, Appl. Catal. A: Gen. 199 (2000) 147–190.
[10] P. Priecel, D. Kubička, L. Čapek, Z. Bastl, P. Ryšánek, Appl. Catal. A: Gen. 397 (2011) 127–137.
[11] O.İ. Şenol, T.R. Viljava, A.O.I. Krause, Catal. Today 106 (2005) 186–189.
[12] O.İ. Şenol, T.R. Viljava, A.O.I. Krause, Appl. Catal. A: Gen. 326 (2007) 236–244.
[13] O.İ. Şenol, E.M. Ryymin, T.R. Viljava, A.O.I. Krause, J. Mol. Catal. A: Chem. 277 (2007) 107–112.
[14] N. Shi, Q.-Y. Liu, T. Jiang, T.-J. Wang, L.-L. Ma, Q. Zhang, X.-H. Zhang, Catal. Commun. 20 (2012) 80–84.
[15] V.A. Yakovlev, S.A. Khromova, O.V. Sherstyuk, V.O. Dundich, D.Y. Ermakov, V.M. Novopashina, M.Y. Lebedev, O. Bulavchenko, V.N. Parmon, Catal. Today 144 (2009) 362–366.
[16] J.-H. Lee, E.-G. Lee, O.-S. Joo, K.-D. Jung, Appl. Catal. A: Gen. 269 (2004) 1–6.
[17] T.V. Reshetenko, L.B. Avdeeva, Z.R. Ismagilov, A.L. Chuvilin, V.A. Ushakov, Appl. Catal. A: Gen. 247 (2003) 51–63.
[18] A.R. Ardiyanti, S.A. Khromova, R.H. Venderbosch, V.A. Yakovlev, H.J. Heeres, Appl. Catal. B: Environ. 117–118 (2012) 105–117.
[19] I.V. Semenova, G.M. Florianovich, A.V. Horoshilov, Corrosion and Protection from Corrosion, Fizmatlit, Moscow, 2002.
[20] H. Alves, U. Heubner, in: T.J.A. Richardson (Ed.), Shreir's Corrosion, Elsevier, Oxford, 2010, pp. 1879–1915.
[21] B. Mile, D. Stirling, M.A. Zammit, A. Lovell, M. Webb, J. Catal. 114 (1988) 217–229.
[22] S.A. Khromova, A.A. Smirnov, O.A. Bulavchenko, A.A. Saraev, V.V. Kaichev, S.I. Reshetnikov, V.A. Yakovlev, Appl. Catal. A: Gen. 470 (2014) 261–270.
[23] M. Saghafi, S. Heshmati-Manesh, A. Ataie, A.A. Khodadadi, Int. J. Refract. Met. Hard Mater. 30 (2012) 128–132.
[24] T. Borowiecki, W. Gac, A. Denis, Appl. Catal. A: Gen. 270 (2004) 27–36.
[25] M.V. Bykova, D.Y. Ermakov, V.V. Kaichev, O.A. Bulavchenko, A.A. Saraev, M.Y. Lebedev, V.A. Yakovlev, Appl. Catal. B: Environ. 113–114 (2012) 296–307.
[26] V.V. Kaichev, A.Y. Gladky, I.P. Prosvirin, A.A. Saraev, M. Hävecker, A. Knop-Gericke, R. Schlögl, V.I. Bukhtiyarov, Surf. Sci. 609 (2013) 113–118.
[27] G. Moretti, J. Electron Spectrosc. Relat. Phenom. 76 (1995) 365–370.
[28] V.I. Bukhtiyarov, I.P. Prosvirin, E.P. Tikhomirov, V.V. Kaichev, A.M. Sorokin, V.V. Evstigneev, React. Kinet. Catal. Lett. 79 (2003) 181–188.
[29] S. Mentus, B. Tomić-Tucaković, D. Majstorović, R. Dimitrijević, Mater. Chem. Phys. 112 (2008) 254–261.
[30] W.-Y. Wang, Y.-Q. Yang, J.-G. Bao, H.-A. Luo, Catal. Commun. 11 (2009) 100–105.
[31] O.İ. Şenol, T.R. Viljava, A.O.I. Krause, Catal. Today 100 (2005) 331–335.
[32] L. Chen, Y. Zhu, H. Zheng, C. Zhang, B. Zhang, Y. Li, J. Mol. Catal. A: Chem. 351 (2011) 217–227.
[33] J. Monnier, H. Sulimma, A. Dalai, G. Caravaggio, Appl. Catal. A: Gen. 382 (2010) 176–180.
[34] S. Tada, T. Shimizu, H. Kameyama, T. Haneda, R. Kikuchi, Int. J. Hydrogen Energy 37 (2012) 5527–5531.
[35] I. Graça, L.V. González, M.C. Bacariza, A. Fernandes, C. Henriques, J.M. Lopes, M.F. Ribeiro, Appl. Catal. B: Environ. 147 (2014) 101–110.
[36] R. Pestman, R.M. Koster, J.A.Z. Pieterse, V. Ponec, J. Catal. 168 (1997) 255–264.
[37] R. Pestman, R.M. Koster, A. van Duijne, J.A.Z. Pieterse, V. Ponec, J. Catal. 168 (1997) 265–272.
[38] V.M.L. Whiffen, K.J. Smith, Energy Fuels 24 (2010) 4728–4737.
[39] W. Wang, Y. Yang, H. Luo, T. Hu, W. Liu, Catal. Commun 12 (2011) 436–440.